applied sciences

MDPI

Article

Characterization of the Products of the Catalytic Pyrolysis of Discarded COVID-19 Masks over Sepiolite

Francisco Ortega [1], María Ángeles Martín-Lara [1,*], Héctor J. Pula [2], Montserrat Zamorano [3], Mónica Calero [1,*] and Gabriel Blázquez [1]

[1] Chemical Engineering Department, Faculty of Sciences, University of Granada, 18071 Granada, Spain
[2] Aula del Mar CEI.Mar UGR, 18071 Granada, Spain
[3] Civil Engineering Department, Higher Technical School of Roads, Canals and Ports, University of Granada, 18071 Granada, Spain
* Correspondence: marianml@ugr.es (M.Á.M.-L.); mcaleroh@ugr.es (M.C.)

Abstract: This research aims to develop a new strategy to valorize wasted COVID-19 masks based on chemical recycling by pyrolysis to convert them into useful products. First, surgical and filtering face piece masks, as defined in Europe by the EN 149 standard (FFP2), were thermally pyrolyzed at temperatures of 450, 500, and 550 °C, and the yields of valuable solid (biochar), liquid (biooil), and syngas products and their characteristics were determined. At low temperatures, biochar formation was favored over biooil and syngas production, while at high temperatures the syngas product yield was enhanced. The highest yield of biooil was found at a pyrolysis temperature of 500 °C, with both surgical and FFP2 masks achieving biooil yields of 59.08% and 58.86%, respectively. Then, the pyrolysis experiments were performed at 500 °C in a two-stage pyrolysis catalytic reactor using sepiolite as a catalyst. Sepiolite was characterized using nitrogen adsorption–desorption isotherms and Fourier-transform infrared spectroscopy. Results showed that the two-stage process increased the final yield of syngas product (43.89% against 39.52% for surgical masks and 50.53% against 39.41% for FFP2 masks). Furthermore, the composition of the biooils significantly changed, increasing the amount of 2,4-Dimethyl-1-heptene and other olefins, such as 3-Eicosene, (E)-, and 5-Eicosene, (E)-. Additionally, the methane and carbon dioxide content of the syngas product also increased in the two-stage experiments. Ultimately, the effect of sepiolite regeneration for its use in consecutive pyrolysis tests was examined. Characterization data showed that, the higher the use-regeneration of sepiolite, the higher the modification of textural properties, with mainly higher changes in its pore volume. The results indicated that the pyrolysis of face masks can be a good source of valuable products (especially from biooil and syngas products).

Keywords: pyrolysis; catalyst; COVID-19 waste; plastic waste; sepiolite

Citation: Ortega, F.; Martín-Lara, M.Á.; Pula, H.J.; Zamorano, M.; Calero, M.; Blázquez, G. Characterization of the Products of the Catalytic Pyrolysis of Discarded COVID-19 Masks over Sepiolite. *Appl. Sci.* **2023**, *13*, 3188. https://doi.org/10.3390/app13053188

Academic Editor: Hyun-Seog Roh

Received: 4 February 2023
Revised: 27 February 2023
Accepted: 28 February 2023
Published: 2 March 2023

1. Introduction

The global pandemic situation declared in 2020 due to the disease called COVID-19 and government measures to avoid its spread caused a dramatic increase in the consumption of face masks, gloves, and other single-use plastic-based personal protective equipment (PPE) [1]. As a result of the high demand and elevated consumption of these single-use plastic-based materials, a great amount of waste is produced, with a monthly estimation of 129 billion face masks and 65 billion gloves globally [2,3]. Spain was among the countries with the strictest national lockdown measures in the European Union (EU) during the first wave of the pandemic. After that, the different autonomous communities applied different restriction regimes. The use of masks was encouraged in public spaces and, in some instances, was imposed in public transport. Therefore, in Spain, the COVID-19 pandemic had a noticeable effect on the manufacturing of personal protective products by the Spanish manufacturing industry, due to the strong demand of them by the population.

Thus, in 2020, more than 293 million masks were sold. About 265.4 million surgical masks, 27.6 million masks with filtering polymeric fibrous materials (FPP filters), almost 8 million protection screens, and 85,545 tons of hand sanitizer gels were sold. The values of these sales were EUR 149 million in masks, EUR 18 million in screens, and EUR 296 million in gels [4]. As a consequence, the development and application of appropriate eco-friendly methods of management of PPE waste is especially valuable [5].

PPE is made of different types of polymers; even the same equipment has several types of plastic in its structure. For example, surgical masks are usually made of three layers of polypropylene, with nylon ear straps and a metal nose clip wrapped in polyethylene [6]. This factor, coupled with the possible presence of micro-organisms, causes this class of waste requires special treatment [7]. Incineration is currently one of the most widespread methods for the treatment of healthcare waste. However, the combustion gases not only discharge greenhouse gas emissions into the environment but can also release toxic substances, such as dioxins and furans, that need to be properly treated, or particulate matter [8,9]. Landfilling is another of the most common approaches extensively applied to discard PPE. Nevertheless, there are some important drawbacks to this method. First, since the PPE degrades slowly, the generated toxic substances stay in the air/water/soil for an extended period [10]. Furthermore, landfilling needs a massive space. Therefore, to address the challenges in PPE waste management, different researchers are now working on advanced technologies, such as glycolysis, hydrogenation, hydrolysis, pyrolysis, and gasification to transform PPE into value-added products [11]. Of these approaches, pyrolysis is one of the best techniques for the valorization of PPE due to its high economic viability and technical feasibility [12]. This technique has been commercially used for plastic upcycling by some petrochemical companies worldwide [13]. It consists of the use of thermal energy in an oxygen-free environment to break the chemical bonds of plastic polymers to obtain three valuable products: biooil, syngas, and biochar, which can play an essential role in industries and refineries [9,14,15]. The yield and properties of products is strongly influenced by various operating parameters including temperature, heating rate, or usage or not of catalysts, among others.

To upgrade the primary products obtained from pyrolysis of plastic waste, different catalysts have been explored. In particular, the effect of several types of zeolite catalysts on the yields of biochar, biooils, and gases has been extensively investigated [16]. Other works includes the use of different metal oxides (Al_2O_3, Fe_2O_3, CeO_2, MoO_3, TiO_2, etc.) as catalyst [17,18]. These catalysts efficiently reduce the temperature needed for breaking and transform the product yield and composition [11]. Although commercial catalysts display stability and easy recyclability, their high cost is one of the main limitations for large-scale plastic waste recycling. A potential solution to this limitation can be replacing them with low-cost materials without supply problems. In this sense, local clay and clay-based materials are good candidates as low-cost catalysts for plastic waste pyrolysis [19].

In the case of PPE waste, some previous studies have reported the valorization by pyrolysis of different types of PPE, including PPE components [20,21], complete PPE [22,23], combinations of different PPE, such as face masks and gloves [24], or co-pyrolysis of PPE and other type of waste, such as food waste [25]. Some studies have performed experiments in thermobalance and have obtained kinetic parameters for different masks [26–28]. Other authors have also conducted computer simulations for the thermal conversion of face masks by pyrolysis [27]. Furthermore, Ali et al. [29] examined the conversion of surgical masks into useful products using metal oxides (CeO_2 and Nb_2O_5) as catalysts. These authors constructed a detailed kinetic model that can be useful to industrial pyrolysis reaction units for the recycling of the face mask waste. Lee et al. [30] have also analyzed the catalytic pyrolysis of face masks by using zeolite catalysts to produce benzene, toluene, ethylbenzene, and xylene (BTEX) compounds. Other researchers have oriented their investigation to the development of porous carbon materials from face masks for energy storage applications (lithium sulfur batteries [31] or supercapacitors [32]). More recently, Wang et al. [13] have analyzed the applicability of the hydropyrolysis and hydrocracking processes to convert

face masks into fuel-range iso-alkanes using Ru/C as a catalyst. Ramalingam et al. [33] examined the thermal pyrolysis of different medical waste including face masks, gloves, and other PPE waste with a special emphasis on the characteristics of the obtained liquid product. The authors concluded that the fuel properties of the liquid product from pyrolysis of face masks, gloves, and other PPE waste were closer to diesel fuel.

However, to the best of our knowledge, clay and clay-based materials were not studied in catalytic pyrolysis of any PPE waste. Therefore, in this study, the thermal and catalytic pyrolysis over an abundant Spanish clay of surgical masks and FFP2 masks was investigated in-depth. Sepiolite clay was chosen because, although it does not contain active components (it is a fibrous hydrated magnesium silicate), it has received considerable attention in catalysis as a support as well as a catalyst [34]. In addition, it is characterized by a highly specific surface area, and water and other inorganic and organic molecules can be accommodated in the sepiolite structure and react between them [35–38]. Some of the main advantages of using sepiolite as a catalyst are its natural origin, low cost (price between 32 and 1000 USD/t in the function of application and processing), and high availability in Spain (Spain is one of the main world producers of sepiolite) [39].

First, the influence of pyrolysis temperature and the interaction of sepiolite on the yields and composition of pyrolysis products (biochar, biooil, and syngas) were studied in a typical pyrolysis temperature range (450–550 °C). Then, the regeneration of the sepiolite was evaluated in three consecutive pyrolysis cycles. The results will support the applicability of this new route of management for PPE that aims to mitigate plastic contamination caused by inadequate management and to achieve sustainable upcycling of waste to high value-added by-products in the future.

2. Materials and Methods

2.1. Materials and Characterization

Biologically uncontaminated disposable surgical and FFP2 masks were collected after regular use. Prior to pyrolysis tests, the composition of the masks was identified by Fourier-transform infrared spectroscopy (FTIR), using a Perkin-Elmer Spectrum 65 spectrophotometer. For this, the masks were separated into their layers, as shown in Figure 1. The surgical mask contains three layers, and the FFP2 mask contains five layers. In addition, both masks contain a nose bridge and ear straps, which are discarded.

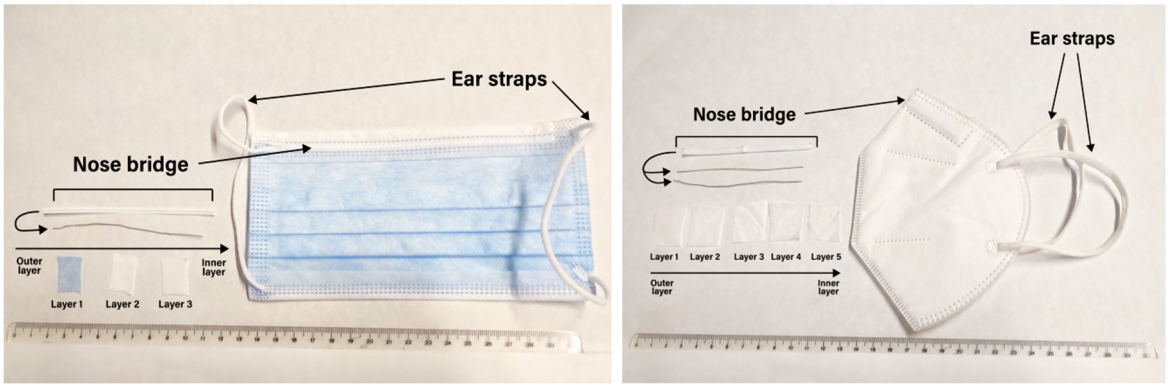

Figure 1. A photograph of the mask separated into its different parts: surgical mask (**left**), FFP2 mask (**right**).

The proximate analysis (moisture, ash, and volatile matter) was determined using the standards ISO 21660-3:2021, ISO 21656:2021, and ISO 22167:2021, while fixed carbon content was evaluated on the difference basis (100-moisture-ash-volatile matter). The elemental content was analyzed using an elemental analyzer (TruSpec Micro CHNS). Finally, the FTIR spectra were obtained using a Perkin-Elmer (Waltham, MA, USA), (model Spectrum 65) spectrometer between 4000 and 400 cm^{-1}.

The catalyst used in the pyrolysis experiments was sepiolite provided by Sigma-Aldrich (St. Louis, MO, USA). Prior to the pyrolysis test, the catalyst was calcined at 550 °C for 3.5 h in an air atmosphere. The surface properties of the catalyst were measured using N_2 adsorption at 196 °C on Micromeritics ASAP 2020 equipment. The specific surface area was calculated according to the BET equation. The T-plot method and BJH method were used to obtain the total pore volume and average pore size distribution, respectively. Furthermore, the IR spectrum of the catalyst was obtained using a Perkin-Elmer Spectrum 65 spectrophotometer. The strength of active site measurement on the surface of the catalytic materials was carried out by temperature-programmed ammonia desorption under helium flow (50 mL/min) from room temperature to 500 °C with a 30 °C/min heating gradient over approximately 0.085 g of sample on a chemisorption analyzer AutoChem II 2920 model from the Micrometrics Instrument Corporation (Norcross, GA, USA), provided with a thermal conductivity detector. Before the chemosorption, the samples were pretreated at 450 °C under He flow for one hour and then cooled to room temperature. Chemisorption was performed using a mixture of ammonia and helium at 10% for 20 min.

2.2. Pyrolysis Experiments

The pyrolysis and catalytic pyrolysis were carried out in a horizontal tubular furnace with integrated control systems provided by Nabertherm with a length of 450 mm and an inner diameter of 50 mm. The schematic layout of the experimental setup is shown in Figure 2.

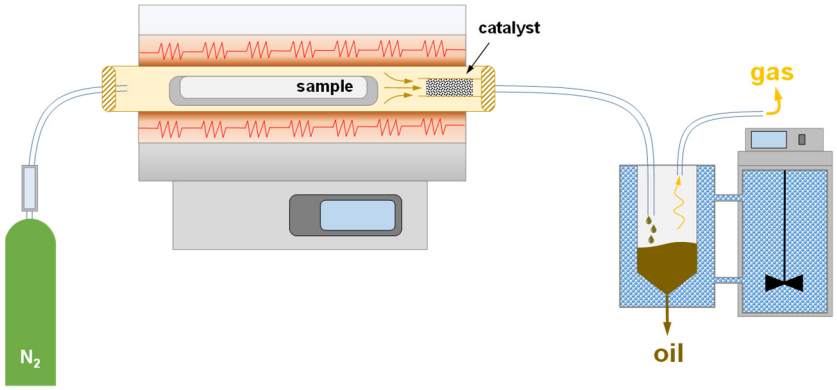

Figure 2. Pyrolysis experimental installation.

First, 15.0 g of sample cut into 10–20 mm pieces was used in an inert N_2 atmosphere. It is important to underline that only layers and ear straps were chosen for pyrolysis tests. The nose bridge was separated from the samples. Once the sample has been weighed, the reactor is started, and the nitrogen flow rate is regulated to 50 L/h. The sample is introduced when no oxygen is left in the oven, and it starts heating with a heating rate of 10 °C/min until the test temperature (450–550 °C) is reached. Once the temperature is arrived at, a residence time in the furnace of 60 min is programmed. To collect the liquids (biooils) generated, two glass traps, submerged in a bath of water, ice, and salt, are placed at the outlet of the tubular reactor. The volatiles that do not condense pass through the pipe and end up filling a hermetic gasbag to constitute the gaseous fraction. Each bag is filled for 15 min, for a total of four bags. After the experiment has been completed, the biooil is weighed, and biooil yield is calculated using Equation (1). The biochar is weighted when the reactor is cooled to room temperature, and biochar yield is obtained using Equation (2). Syngas yield is determined by applying the mass balance to the system (Equation (3)). Equations (1)–(3)are as follows:

$$Oil\ Yield\ (\%) = \frac{M_O}{M_S} \cdot 100 \quad (1)$$

$$Biochar\ Yield\ (\%) = \frac{M_C}{M_S} \cdot 100 \quad (2)$$

$$Syngas\ Yield\ (\%) = 100 - (Oil\ Yield\ (\%) + Char\ Yield\ (\%)) \quad (3)$$

where M_S is the mass of the sample; M_O is the mass of biooil; M_C is the mass of biochar.

In the catalytic pyrolysis experiments, the catalyst was placed ex situ with 5% of the sample mass. Catalyst was mixed with glass balls to prevent clogging. The catalyst was placed at the outlet of the furnace so that the volatiles were in contact with the catalyst. From this point, the catalytic pyrolysis operating procedure was the same as the standard pyrolysis experiment performed at 500 °C (the temperature that provided higher liquid product yields). Once the experiment was over and the reactor reached room temperature, the catalyst was recovered. Fractions yields were obtained using Equations (1)–(3). Finally, the catalyst was calcined at 550 °C for 3.5 h in air atmosphere to regenerate the catalyst and then it was kept free of moisture until the next run.

Three tests were carried out with the catalyst, and after each use the catalyst was treated as indicated above. In addition, the surface properties of the catalyst after each use were determined using N_2 adsorption at 196 °C on a Micromeritics ASAP 2020, and we determined the infrared spectrum using a Perkin-Elmer spectrophotometer, model Spectrum 65.

In addition, all test were performed in triplicate and mean values have been shown.

2.3. Characterization of Liquid Fraction

The compounds in the liquid product were identified by gas chromatography (GC) coupled with mass spectrometry (MS) (Agilent 7890A/Waters Quattro MicroGC). The carrier gas was He with a flow of 1 mL/min, the split ratio was 50:1, the injection volume was 1 µL, and the injector temperature was 240 °C while operating in split mode. The GC column was a nonpolar phase ZB-5MS capillary column, Phenomenex (Torrance, CA, USA), (30 m × 0.25 mm, ID × 0.25 µm film). The oven was programmed from 42 °C to 320 °C at a rate of 6 °C/min and then maintained at 320 °C for 4 min. The standard mass spectral library (NIST MS Search 2008) was used as a reference to identify organic compounds.

The average molecular weight (MW) of the biooil was estimated from the elemental composition of the components detected by GC–MS and the area represented by each compound. Equation (4) is as follows:

$$Average\ MW\ (g/mol) = \sum_1^n x_i \cdot MW_i \quad (4)$$

where MW_i is the molecular weight of component I, and x_i is the area of component i.

Finally, physicochemical characterization of biooil was performed by following the Archimedes' principle (Ohaus's density kit) for density determination. An ASTM D445 and Malvern Kinexus rheometer using a flat plate of 20 mm diameter were used for for viscosity determination, and a pH-meter (HANNA Instruments, Singapore) was used for pH value determination.

2.4. Characterization of Solid Fraction (Biochar)

The elemental content of the biochar was analyzed using an elemental analyzer (TruSpec Micro CHNS). A total of 5 mg of sample was grinded to powder size and sealed in a tin capsule. The C, N, H, and S contents in the sample were detected directly. In the combustion reactor, organic and inorganic compounds are converted into elemental gases that are reduced and separated in a chromatographic column and sent to a thermal conductivity detector.

The energy content of the biochar, high heating value (HHV), was calculated using Equation (5) according to the methods compiled by Kasar and Ahmaruzzaman [34], and based on the results obtained from the elemental analysis. Equation (5) is as follows:

$$HHV\ (MJ/kg) = 0.328 \cdot C + 1.419 \cdot H + 0.0928 \cdot S \quad (5)$$

where C is the carbon content of the sample, wt %, H is the hydrogen content of the sample, wt %, and S is the sulfur content of the sample, wt %.

Finally, the surface properties of the biochar were determined using N_2 adsorption at 196 °C on a Micromeritics ASAP 2020, following the same procedure indicated for the catalyst.

2.5. Characterization of Syngas Fraction

The analysis of non-condensable gases was carried out with a gas chromatograph Agilent 990 equipped with two channels for separation and detection and a micro-machined thermal conductivity detector. The equipment incorporates an MS5A SS 20MX0.25MMX30UM BF RTS column that can be used for the separation of many permanent gas components, such as oxygen, nitrogen, carbon monoxide, or methane, and a PORAPLOT QUM10MX0.25MMX8UM BF column that allows for the determination of components, such as ethane, ethylene, carbon dioxide, propane, n-butane, acetylene, and methyl acetylene.

The energy content of the syngas, high heating value (HHV), was calculated using Equation (6) according to the data compiled in the NIST Web Book and based on the results obtained from the gas chromatography. Equation (5) is as follows:

$$HHV = \sum_1^n \frac{x_i \cdot \Delta cH^\circ gas_i \cdot P}{R \cdot T} \quad (6)$$

where,

HHV is the high heating value, MJ/m^3;
x_i is the molar fraction of component i;
$\Delta cH^\circ gas_i$ is the standard enthalpy change in combustion of component I, MJ/mol;
R is the universal gas constant, m^3·Pa/K·mol;
T is the temperature of the gas, K;
P is thep ressure of the gas, Pa.

3. Results and Discussions

3.1. Characterization of the Face Masks

Before pyrolysis, the analysis of face masks was performed. Table 1 shows a summary of elemental and proximate analysis of surgical and FFP2 masks. These masks contain mainly carbon and hydrogen with a percentage of 81.4 and 15.9 for the FFP2 mask and a percentage of 83.2 and 8.4 for the surgical mask, respectively. No presence of sulfur and nitrogen was found in the mask, and oxygen content (obtained by difference including ash content) was 2.8% and 2.1% for the surgical and FFP2 mask, respectively. Regarding proximate analysis, the ash content is higher for the surgical mask (5.6%) than for the FFP2 mask (0.6%). The percentage of volatiles is very high (>90% in both masks), and the percentage of fixed carbon is low (<4%). These results are like those found by other authors [40,41].

Table 1. Proximate and elemental analysis of the two masks.

		Surgical Mask	FFP2 Mask
Proximate analysis (%)	Moisture	0.3	4.6
	Volatile matter	90.4	92.9
	Fixed carbon	3.7	1.9
	Ash	5.6	0.6
Elemental analysis (%)	Carbon	83.2	81.4
	Hydrogen	8.4	15.9
	Nitrogen	- - -	- - -
	Sulfur	- - -	- - -
	Oxygen	2.8	2.1

The FTIR spectra of the different layers for the surgical and FFP2 mask are shown in Figures 3 and 4, respectively.

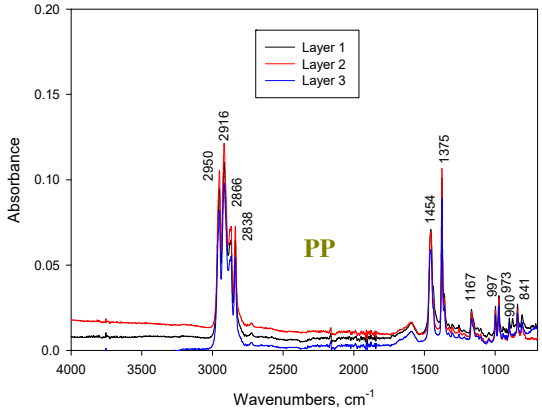

Figure 3. FTIR spectra of the different layers of the surgical mask.

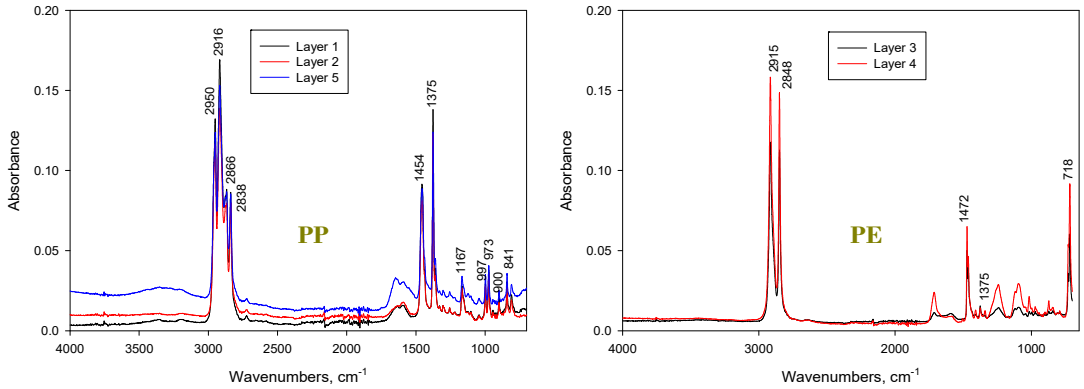

Figure 4. FTIR spectra of the different layers of the FFP2 mask.

Layers 1, 2, and 3 of the surgical masks show identical peaks in the range of 2938 to 2950 cm^{-1} and in the range of 841 to 1454 cm^{-1}. These peaks are characteristic of the polypropylene (PP) FTIR spectrum, so this mask contains three layers of this material. However, FFP2 masks have two types of spectra. Layers 1, 2, and 5 have a spectrum that is practically identical to that of surgical masks, that is, these layers correspond to polypropylene. On the other hand, layers 3 and 4 present a spectrum with peaks characteristic of polyethylene (PE), highlighting the peaks at 2915, 2848, 1472, 1375, and 718 cm^{-1} [18]. Therefore, the FFP2 mask contains five layers, three of polypropylene and two of polyethylene.

Regarding assignation to functional groups, the most prominent peaks of polypropylene are assigned to asymmetric stretching of CH_3 (2950 cm^{-1}), asymmetric stretching of CH_2 (2916 cm^{-1}), CH_3 stretching (2866 cm^{-1}), CH_3 symmetric bending (1454 cm^{-1} and 1375 cm^{-1}), C-H wagging and CH_3 rocking vibration (1167 cm^{-1}), CH_3 rocking vibration and C-C stretching (997 cm^{-1} and 973 cm^{-1}), and C-H rocking vibration (841 cm^{-1}) [42].

Furthermore, the most prominent peaks of the polyethylene layers of the FFP2 masks, which are 2915 cm^{-1}, 2848 cm^{-1}, 1472 cm^{-1}, 1375 cm^{-1}, and 718 cm^{-1}, correspond to CH_2 asymmetric stretching, CH_3 symmetric stretching, bending deformation, CH_3 symmetric deformation, and split CH_2 rocking deformation, respectively [43].

3.2. Thermal Pyrolysis

The yields of the syngas, biooil, and biochar of the thermal pyrolysis of surgical and FFP2 masks at different temperatures are shown in Figure 5.

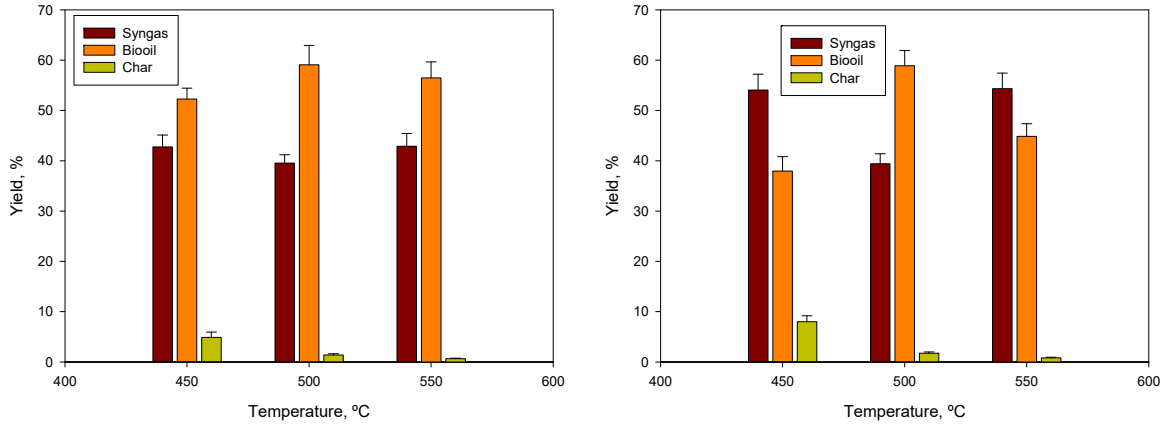

Figure 5. Thermal pyrolysis yields of surgical masks (**left**) and FFP2 masks (**right**).

The results indicate that temperature significantly affects the fractions obtained. The biochar yield decreases with temperature from 4.99% at 450 °C to 0.67% at 550 °C for surgical masks and from 8.02% at 450 °C to 0.82% at 550 °C for FFP2 masks. For both materials, the maximum biooil yield is reached at 500 °C, and the maximum syngas yield at 550 °C. In general, an increase in the pyrolysis temperature promotes cracking reactions, favouring the formation of liquid and gaseous fractions, and reducing the formation of biochar. These results are like those obtained by other researchers. Li et al. [20], studying the pyrolysis of surgical masks, found a decrease in biochar production from 97.6% to 3.9% when the pyrolysis temperature increased from 350 to 500 °C. The percentage of biooil and syngas increases from 1.0 to 80.6% and from 1.4% to 15.5% in the same temperature variation. Sun et al. [6] studied the pyrolysis of masks in a fixed-bed reactor and found that the yields of liquid and gaseous products increase when the pyrolysis temperature is higher in a range of 400 to 580 °C. The percentage of solid drops significantly when the temperature increases from 400 to 440 °C, to remain practically constant. The authors conclude that the results indicate that the pyrolysis of the mask is complete at 440 °C and that a higher temperature produces partial cracking of the heavier volatiles.

3.3. Catalytic Pyrolysis

3.3.1. Effect of Sepiolite on Product Yield

The yields of the syngas, biooil, and biochar of catalytic pyrolysis of surgical and FFP2 masks at different runs are shown in Figure 6. As other authors reflect, in general, the use of a catalyst in masks pyrolysis increased the amount of syngas at the expense of biooil [30,44]. It is especially notable with FFP2 masks, where syngas yield changed from 39.41% to 52.19%. Sepiolite, as catalyst, having acidic sites on it (total acid sites of 0.29 mmol/g, weak acid sites of 0.10 mmol/g) can speed up the dehydration, decarboxylation, and hydrogenation reactions that occur during pyrolysis. Hence, the main role of sepiolite in the product yield is enhancing the ability of the reaction to crack the polymer mask, increasing the cracking mechanism to convert the liquid product into syngas. After each catalyst use, similar syngas and liquid yields were obtained. This is probably due to the good catalyst regeneration and poor catalyst internal structure variation, as will be discussed later in Section 3.3.5. If surface acidity and other surface properties are maintained during regeneration, the potential of secondary reaction, such as an over-cracking mechanism, is similar, so similar product yield distributions are achieved [45]. On the other hand, there are no significant changes in the solid yield results obtained in thermal pyrolysis and catalytic pyrolysis. Only a low variation from 1.39% to 3.91% without a specific trend was observed.

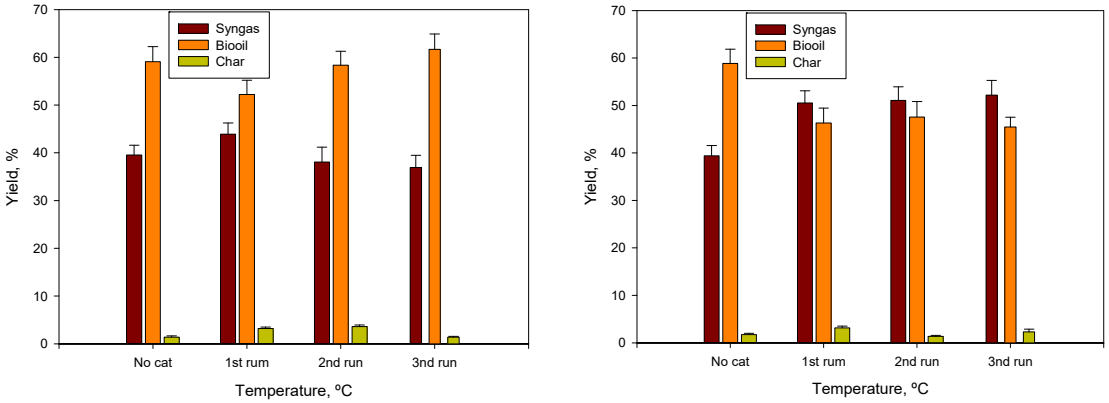

Figure 6. Comparative pyrolysis yields of surgical masks (**left**) and FFP2 masks (**right**).

3.3.2. Characterization of Liquid Fraction

Tables 2 and 3 shows the most common compounds in the recovered biooil after the pyrolysis experiment for surgical and FFP2 masks, respectively. As other authors detailed [23,30,46,47], the major compound recovered was 2,4-Dimethyl-1-heptene during the thermal pyrolysis of masks (>10%). Furthermore, cembrane, 3-Eicosene, (E)-, 5-Eicosene, (E)-, and 1,2-Epoxyhexadecane appeared in a concentration greater than 3% in thermal pyrolysis biooils from face masks.

The use of sepiolite as a catalyst altered the composition of the pyrolysis liquids, significantly increasing the amount of 2,4-Dimethyl-1-heptene and other olefins, such as as 3-Eicosene, (E)- and 5-Eicosene, (E)- at the expense of naphthenes, such as cembrane. Nevertheless, the successive use of the catalyst had the opposite effect on the results obtained, reducing the quantity of light olefins as 2,4-Dimethyl-1-heptene and increasing the proportion of naphthenes, such as 1,2-Epoxyhexadecane. This behavior could be explained due to the degradation experienced by the catalyst, which reduced its micropore area and the total pore volume.

Table 2. Liquid components list in biooil from the pyrolysis of surgical masks.

Component List	Type of Pyrolysis							
	Thermal		Catalytic-1st Run		Catalytic-2nd Run		Catalytic-3rd Run	
	Component	Area, %	Component	Area, %	Component	Area, %	Component	Area, %
1st	2,4-Dimethyl-1-heptene	12.27	2,4-Dimethyl-1-heptene	40.56	2,4-Dimethyl-1-heptene	26.16	2,4-Dimethyl-1-heptene	11.12
2nd	Cembrane	5.59	3-Eicosene, (E)-	10.97	3-Eicosene, (E)-	7.13	1,2-Epoxyhexadecane	6.46
3rd	3-Eicosene, (E)-	4.48	5-Eicosene, (E)-	6.22	1,2-Epoxyhexadecane	5.46	3-Eicosene, (E)-	5.73
4th	1,2-Epoxyhexadecane	4.11	3-Tetradecene, (E)-	4.01	1,7-Dicyclopentyl-4-n-octylheptane	5.15	1,7-Dicyclopentyl-4-n-octylheptane	4.06
5th	1,7-Dicyclopentyl-4-n-octylheptane	3.46	1,3,5-Trimethylcyclohexane	3.60	Cembrane	4.66	Hexadecyl trichloroacetate	3.67

Table 3. Liquid components list in biooil from the pyrolysis of FFP2 masks.

Component List	Type of Pyrolysis							
	Thermal		Catalytic-1st Run		Catalytic-2nd Run		Catalytic-3rd Run	
	Component	Area, %	Component	Area, %	Component	Area, %	Component	Area, %
1st	2,4-Dimethyl-1-heptene	30.26	2,4-Dimethyl-1-heptene	35.71	2,4-Dimethyl-1-heptene	31.61	2,4-Dimethyl-1-heptene	29.61
2nd	1-Decene	6.47	3-Eicosene, (E)-	11.35	3-Eicosene, (E)-	11.75	3-Eicosene, (E)-	12.01
3rd	1,2-Epoxyhexadecane	6.32	5-Eicosene, (E)-	6.42	5-Eicosene, (E)-	6.73	1,2-Epoxyhexadecane	8.01
4th	Cembrane	5.78	1,2-Epoxyhexadecane	5.47	1,2-Epoxyhexadecane	5.88	5-Eicosene, (E)-	7.11
5th	5-Eicosene, (E)-	5.24	Hexadecyl trichloroacetate	3.91	Hexadecyl trichloroacetate	4.36	Hexadecyl trichloroacetate	5.09

Moreover, the components of the biooil obtained have been grouped by the most usual functional groups. Table 4 shows the distribution by functional groups of the biooils. No aromatic compounds have been detected in the biooil from thermal pyrolysis, which coincides with other researchers [30]. However, aromatic compounds have not been found in the biooil obtained in sepiolite-catalyzed pyrolysis, in contrast to other researchers in zeolite-catalyzed pyrolysis [30,47]. In addition, it was observed that through catalytic pyrolysis, the number of olefins and isoparaffins obtained increased to the detriment of naphthenes and paraffins. However, with successive use of the catalyst, it is seen that this trend is reversed due to the degradation that occurs during use. Table 4 also shows that, for all samples, the olefin content was higher than other components, with values around 41–72%, while aromatic compounds were not found.

Table 4. Liquid biooil composition by components groups.

Type of Pyrolysis		Main Component Groups				
		Paraffin	Isoparaffin	Naphthene	Olefin	Others
Surgical mask	Thermal	0.34%	2.19%	16.38%	43.01%	38.07%
	Catalytic-1st run	0.00%	5.15%	3.81%	71.82%	19.22%
	Catalytic-2nd run	0.68%	1.72%	9.08%	42.15%	46.37%
	Catalytic-3rd run	0.76%	2.98%	11.24%	41.35%	43.67%
FFP2 mask	Thermal	0.00%	2.88%	10.64%	56.68%	29.80%
	Catalytic-1st run	0.00%	3.22%	6.39%	64.33%	26.06%
	Catalytic-2nd run	0.00%	2.91%	5.33%	62.54%	29.22%
	Catalytic-3rd run	0.00%	1.69%	8.00%	60.44%	29.87%

On the other hand, biooil compounds were grouped by chain size, and the average MW of the biooil was calculated using Equation (4) (Table 5). It can be noticed that in catalytic pyrolysis (first run) compared to thermal pyrolysis, the biooil obtained has a lower chain size and lower average molecular weight. In contrast, the successive use of the catalyst has the opposite effect, increasing the chain size and the average molecular weight of the biooil, even reaching higher values than in thermal pyrolysis.

Regarding the mechanism of pyrolysis, in polymers, such as polypropylene and polyethylene, the main constituents of face masks, the thermal decomposition process occurs by radical chain reactions and hydrogen transfer steps that gradually break the main chain through the elimination of small molecules. The mechanism has been previously discussed by other authors [48–53].

Frequently in catalytic pyrolysis, the first step consists of the protonation of carbon atoms to form carbocations that can be stabilized by β fission reactions, isomerization, or hydrogen transfer [54]. The protonation of carbon to form carbocations occurs when protons are donated by the Brønsted acid sites or the capture of a hydride through the Lewis acid sites [54–56]. In the case of sepiolite and other clay minerals, their acidity probably

comes from the dissociation of the water that is coordinated with cations located between the clay layers (Brønsted acidity) [52].

Table 5. Liquid biooil composition by chain size and average molecular weight.

Type of Pyrolysis		Chain Size			Average MW of Biooil (g/mol)
		C 5–9	C 9–13	C +13	
Surgical Mask	Thermal	27.4%	8.2%	64.4%	271.4
	Catalytic-1st run	50.5%	12.1%	37.4%	186.8
	Catalytic-2nd run	32.7%	11.0%	56.3%	230.9
	Catalytic-3rd run	22.6%	12.3%	65.1%	259.3
FFP2 Mask	Thermal	38.6%	15.4%	46.0%	211.8
	Catalytic-1st run	42.8%	9.2%	48.1%	207.5
	Catalytic-2nd run	38.5%	10.0%	51.4%	214.0
	Catalytic-3rd run	32.3%	12.0%	55.7%	228.5

Finally, some data about the physicochemical characterization of biooil simples was also provided in Table 6. The viscosity of the biooil obtained from the thermal pyrolysis of the surgical mask was 4.09 cSt, comparable to diesel fuel. However, the viscosity of the thermal pyrolysis of FFP2 masks was very high (154.49 cSt). Viscosity plays an important role in the use of biooil as fuel. The high viscosity of biooil from FFP2 masks has a negative influence on fluidity, which, for example, may cause engine damage during combustion and difficulty in the transportation in pipelines due to the friction against the pipe walls that, in addition, can result in more pumping power consumption [57]. Regarding density, both surgical and FFP2 masks provided densities between 790 and 800 kg/m^3, similar to diesel and gasoline fuel [28]. Furthermore, the pH of the biooil samples was 6.00. This value can be considered a good pH value, since it is not so acid as to induce corrosion during its application. The most important effect of catalytic pyrolysis on physicochemical properties of biooil simples was observed in the viscosity parameter. Hence, biooil from catalytic pyrolysis of FFP2 masks changed from 154.49 cSt to 15.03 cSt. This important decrease in viscosity could be explained as being due to the formation of simpler components due to cracking. This influences the decrease in the wax content obtained from the biooil product of polyethylene of the FFP2 masks and, consequently, less viscosity for the biooil product was observed.

Table 6. Physicochemical characterization of liquid biooil.

	Surgical Mask		FFP2 Mask	
	Thermal	Catalytic-1st Run	Thermal	Catalytic-1st Run
Density 15 °C (kg/m^3)	810	790	850	830
Viscosity (cSt)	4.09	3.15	154.49	15.03
pH value	6.0	6.1	6.0	5.9

3.3.3. Characterization of Solid Fraction

Table 7 represents the elemental components, the C/N and C/H ratio, and *HHV* of the biochars obtained by thermal and catalytic pyrolysis. In general, the results found are similar for all the biochar samples, which indicate that the use of the catalyst does not have an appreciable influence on the characteristics of the biochar. The *HHV* values are, like the biochar, produced from plastics, such as HDPE [58] and PP [59], and are higher than biochar from municipal solid waste (MSW) mixture [60], plastic mix from MSW mixture [61] and lower than biochar from biomass [62,63]. Regarding elemental composition, a high carbon content was observed (from 50.0 to 70.9%), lower nitrogen (from 1.1 to 5.4%) lower hydrogen (from 3.1 to 9.4%), and no sulfur. Comparing thermal and catalytic pyrolysis, the most notable aspect is the decrease in hydrogen content for both

the FFP2 and surgical masks and the increase in the carbon content for the surgical masks, which could be attributed to a change in the reactions that can occur during the pyrolysis process due to the presence of the catalyst.

Table 7. Solid biochar elemental analysis.

Biochar Samples	Elements, wt. %					C/N	C/H	*HHV*, MJ/kg
	N	C	H	S	O *			
FFP2 mask biochar	5.37	59.81	9.35	0.00	25.47	11.13	6.40	32.88
FFP2 mask (5% sepiolite 1st run) biochar	3.39	56.72	3.25	0.00	36.64	16.73	17.45	23.22
FFP2 mask (5% sepiolite 2nd run) biochar	3.34	56.24	3.17	0.00	37.23	16.84	17.71	22.95
FFP2 mask (5% sepiolite 3rd run) biochar	3.30	55.77	3.10	0.00	37.83	16.90	17.99	22.69
Surgical mask biochar	1.13	50.01	7.53	0.00	41.34	44.26	6.64	27.08
Surgical mask (5% sepiolite 1st run) biochar	2.81	70.92	3.92	0.00	22.35	25.24	18.09	28.82
Surgical mask (5% sepiolite 2nd run) biochar	3.31	69.84	4.16	0.00	22.69	21.13	16.79	28.81
Surgical mask (5% sepiolite 3rd run) biochar	3.80	68.76	4.40	0.00	23.04	18.09	15.63	28.80

* by difference between 100% and CNHS content, %.

Today, the applications of biochar solid are very limited; nevertheless, some emerging uses have been considered. The biochar can be used as low-quality fuel for combustion processes, as a precursor to obtain adsorbents, as additives in epoxy resins, or as crop nutrients, among others [64–69].

The high heating values obtained in this work (Table 5) suggested that biochar can be a stronger candidate for mainly solid fuel use. Furthermore, the values of nitrogen content show the fitness of biochar as a soil enhancer and growth nutrient in crops.

On the other hand, an application also investigated for biochar is its use as solid adsorbent. The potential of biochar for use as adsorbent is based primarily on its surface properties. In this sense, the surface properties of the obtained biochars have been determined. For the FFP2 mask, a BET surface area of 0.235 m^2/g, a total pore volume of 0.011 cm^3/g, and an average pore diameter of 191.6 nm were obtained. For the surgical mask, these values were 4.941 m^2/g, 0.012 cm^3/g, and 9.717 nm, respectively. The low BET surface area values of these biochars are justified by the fact that they have not been subjected to a subsequent activation process, so the presence of residual volatile matter can block the porosity of the biochars [70]. Other researchers also found low BET surface area values for the biochar obtained in the pyrolysis of different plastic waste [61,71–74].

In the recent years, the use of the biochar as a raw material for producing activated materials has been consolidated as an attractive strategy to prepare adsorbents with good adsorption capacities for an important range of pollutants [75].

3.3.4. Characterization of Syngas Fraction

The overall composition of the syngas product is presented in Table 8. Hydrocarbons constitute most of pyrolysis gases. The gases derived from thermal and catalytic pyrolysis of both surgical and FFP2 masks had average hydrocarbon contents between 77.8 and 85.5%. In all tests, the major compound was methane (CH_4) with an average content of 47.9%. The highest volumetric content of CH_4 was observed in gases produced from catalytic pyrolysis of FFP2 masks with values between 50.9% and 52.5% in the function of the number of runs after the regeneration of sepiolite. Another relatively abundant hydrocarbon is ethane, with averages values of 16.0% and 13.2% for gases produced from the pyrolysis of surgical and FFP2 marks, respectively. Especially significant was the decrease in ethane (C_2H_6) content in the catalytic pyrolysis of FFP2 masks and the increase in methane content. Another important hydrocarbon is propane. It was found in low concentrations, while in some catalytic pyrolysis experiments it was not detected. These results agree with some previous

studies [20,23,46] at similar operating conditions. However, other authors determined that the major component in their investigations was propene (C_3H_6) [25,30] and other heavier components [6].

Table 8. Overall composition of the syngas stream.

Sample	*HHV*, MJ/Nm^3	Molar Composition (%)								
		Hydrogen	Methane	Carbon Monoxide	Ethane	Ethylene	Carbon Dioxide	Ethyne	Propane	Propyne
Surgical mask	46.71	0.83	42.84	9.63	15.99	5.07	10.46	0.91	8.20	6.07
Surgical mask + catalyst (1st)	45.65	0.83	46.53	7.63	12.95	4.71	11.42	3.08	6.28	6.57
Surgical mask + catalyst (2nd)	42.31	1.30	46.75	9.29	16.25	5.65	11.61	2.65	0.00	6.50
Surgical mask + catalyst (3rd)	43.50	0.97	45.60	9.20	18.88	5.54	10.56	3.61	0.00	5.65
FFP2 mask	47.12	1.55	46.70	3.59	18.93	8.03	9.37	4.96	1.54	5.34
FFP2 mask + catalyst (1st)	41.95	1.75	52.45	7.37	8.76	8.22	10.62	4.52	0.00	6.31
FFP2 mask + catalyst (2nd)	42.73	0.97	51.50	6.82	12.73	7.83	11.10	2.38	0.00	6.67
FFP2 mask + catalyst (3rd)	42.01	0.76	50.92	8.99	12.27	7.38	10.70	2.74	0.00	6.23

Regarding carbon dioxide (CO_2), it was present in all gases at an average concentration of 11.0% and 10.4% for the gases of the pyrolysis of surgical and FFP2 marks, respectively. It has a negative effect, since it reduces the energy quality of the syngas. Furthermore, carbon monoxide (CO) was present in all gases, although in lower concentrations (between 3.6% and 9.6%). Variations were observed in the function of the type of mask, if the pyrolysis was thermal or catalytic and, in catalytic pyrolysis, the number of runs performed, but a clear tendency was not determined. The presence of oxygenated compounds in the gases may be due to the small amount of oxygen present in the masks, which can be attributed to the presence of other unidentified compounds constituting the different layers of the masks [40]. In addition, it could also be due to the air that inevitably enters during the loading of the material into the reactor. Park et al. [25] also found CO_2 and CO in the gases produced in the pyrolysis of masks at different temperatures. These authors attribute the presence of CO_2 and CO to the thermal cracking of the pyrolytic vapor and the oxygen content in the feed wastes. Thus, the authors studied the pyrolysis of mixtures of masks and food waste and found that the contents of CO_2 and CO in the syngas were proportional to the amount of food waste introduced into the pyrolyzed food waste–mask mixture due to the higher oxygen content in food waste than in masks. Finally, the H_2 content was very low, with values ranging between 0.8% and 1.8%.

In addition, the gases produced from the pyrolysis of masks have high calorific values, higher than 40 MJ/Nm^3 in all cases, with only a slight decrease with the use of the catalyst. Therefore, the gases produced can be used as fuel for different applications, such as the production of electrical energy in combustion engines or gas turbines.

The syngas composition was studied over the duration of the experiment by analyzing its evolution over time. Figures S1 and S2 represent the evolution of gas composition over the time for the pyrolysis experiments. Two clear trends can be observed in the experiments.

On the one hand, in the thermal pyrolysis and in the first use of catalyst in the catalytic pyrolysis of both masks, it is appreciated that methane increases to a maximum at 30 min and then decreases, while ethane has the opposite behavior. In addition, propane increased over time, reaching end values above the methane composition in the surgical mask pyrolysis.

For the second and the third use of the catalyst in catalytic pyrolysis, the highest composition of methane was reached at the end of the experiment at the expense of ethane. The rest of the compounds remained practically stable.

3.3.5. Effect of Regeneration on Sepiolite Properties

Table 9 represents the surface characteristics measured on the catalyst before the pyrolysis and after the third experiment of each feed material. Although there was a decrease in all surface characteristics, especially in the surface micropore area resulting in a reduction of 66–72%, these changes can be the reason for the variations in biooil and syngas yields and in the properties of the obtained products after each use of the catalyst.

Table 9. Catalyst characterization.

	Catalyst (Before Using)	**Used Catalyst (3rd Run) (Surgical Masks)**	**Used Catalyst (3rd Run) (FFP2 Masks)**
BET surface area	138 m^2/g	118 m^2/g	116 m^2/g
Pore volume (<370 Å)	0.3 cm^3/g	0.2 cm^3/g	0.2 cm^3/g
Micropore area	9 m^2/g	3 m^2/g	2 m^2/g
External surface area	129 m^2/g	115 m^2/g	113 m^2/g
Average pore size	2.3 nm	2.0 nm	2.0 nm

In addition, Figure 7 shows the FTIR of the catalyst before pyrolytic tests and after the last pyrolysis regeneration cycle. No important differences were found on the three spectra. The results in Table 9 and Figure 7 indicate the good renewable properties of sepiolite. They agree with the theory that regenerated and reused sepiolite showed practically identical conversion and yield values compared with the fresh catalyst. Absence of bands at 3600–3500 cm^{-1} corresponding to the OH stretching vibration of Mg_3-OH groups, or at 3500–3400 cm^{-1}, 1700–1600 cm^{-1}, and 1500–1400 cm^{-1} corresponding to the silanol bands (Si-OH) and the bending vibrations of the OH that forms part of the water bound to the structure is observed [76,77]. This implies that there is no water present in the structure of calcined sepiolite or after it has been used and regenerated. Only a slight decrease in signal intensity is observed in the bands 1060–1050 cm^{-1} and 900–800 cm^{-1} which are associated with Si-O stretching vibrations [78,79].

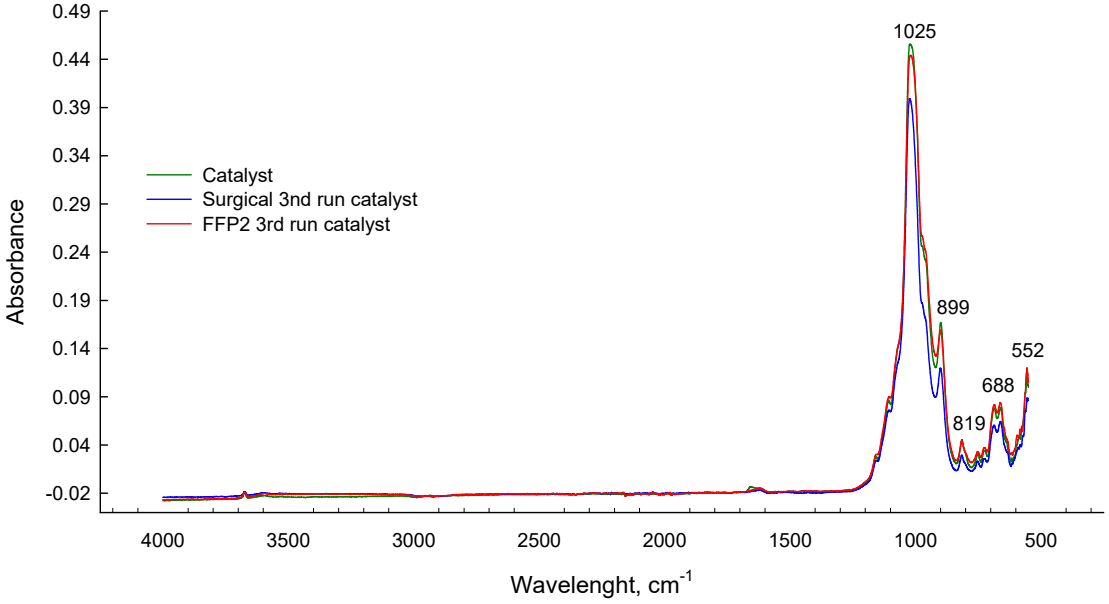

Figure 7. Catalyst FTIR comparison.

4. Conclusions

In this study, the discarded surgical and FFP2 face masks were pyrolyzed as a strategy to produce high value-added by-products from a new increasing waste stream, such as personal protective equipment used against COVID-19. The influence of temperature on the products was studied in a typical pyrolysis temperature range (450–550 °C). Temperature significantly affects the fractions obtained; we found that the highest amount of liquid fraction for the thermal pyrolysis of surgical and FFP2 masks was obtained at 500 °C and the maximum syngas yield was at 550 °C. The percentage of solid drops significantly when the temperature increases from 400 to 440 °C, to remain practically constant.

Furthermore, the interaction of a low-cost catalyst, such as sepiolite, during pyrolysis was investigated. Results showed that, in general, the use of sepiolite increased the amount of syngas at the expense of biooil. Additionally, in catalytic pyrolysis, the olefin and isoparaffin content in biooil obtained increased to the detriment of naphthenes and paraffins. However, with the successive use of the catalyst, it is seen that this trend is reversed due to the degradation that occurs during use. Aromatic compounds were not found in either thermal or catalytic pyrolysis.

Regarding the solid fraction, the results found are similar for all the biochar samples, which indicate that the use of the catalyst does not have an appreciable influence on the characteristics of the biochar. Elemental analysis showed a high carbon content (from 50.0 to 70.9%), lower nitrogen and hydrogen, and no sulfur. The high heating values of the biochar samples obtained in this work suggested that biochar could be used as a solid fuel.

The gases derived from the thermal and catalytic pyrolysis of both surgical and FFP2 masks had average hydrocarbon contents between 77.8 and 85.5% and high calorific values, so they could be used as fuels for different applications. In all tests, the major compound was methane (CH_4), with an average content of 47.9%. In addition, in the thermal pyrolysis and in the first use of the catalyst in the catalytic pyrolysis of both masks, methane increased to a maximum at 30 min and then decreased, while ethane had the opposite behavior. For the second and the third use of catalyst, the highest composition of methane was reached at the end of the experiment at the expense of ethane.

Finally, characteristics measured on the catalyst before and after its use in the pyrolysis test showed that a good regeneration was performed.

Hence, it is concluded that the face mask waste can be used in the pyrolysis processes to convert them into useful products. However, before large-scale application, some additional research is needed to solve the following aspects:

- The construction of detailed kinetic models.
- Understanding of the pyrolysis mechanism over sepiolite to adequately modify this material to develop more selective sepiolite-based catalysts towards specific high-value products.
- The analysis of the socio-economic and environmental impacts.

Supplementary Materials: The following supporting information can be downloaded at: https://www.mdpi.com/article/10.3390/app13053188/s1, Figure S1: Syngas component yield in catalytic pyrolysis of surgical masks. Figure S2: Syngas component yield in catalytic pyrolysis of FFP2 masks.

Author Contributions: F.O.: performed the experiments and collected the experimental data; wrote the original draft of manuscript; M.Á.M.-L.: conceived and designed the experiments; performed the analysis of the data; wrote the advanced versions of the manuscript; funding acquisition; supervision; H.J.P.: revised and edited the final version of the manuscript; M.Z.: revised and edited the final version of the manuscript; M.C.: conceived and designed the experiments; performed the analysis of the data; wrote the advanced versions of the manuscript; funding acquisition; supervision; G.B.: performed the experiments and collected the experimental data; contributed to the analysis of the data; supervision. All authors have read and agreed to the published version of the manuscript.

Funding: This work was supported by project "RECOMAR", reference PYC20 RE 041 UGR, co-financed 80% by the ERDF, ERDF Operational Program 2014–2020 and the Ministry of Economic Transformation, Industry, Knowledge and Universities, Junta de Andalucía. European Union–European Regional Development Fund (ERDF)-"Andalusia moves with Europe".

Institutional Review Board Statement: Not applicable.

Informed Consent Statement: Not applicable.

Conflicts of Interest: The authors declare no conflict of interest.

References

1. Aragaw, T.A. Surgical face masks as a potential source for microplastic pollution in the COVID-19 scenario. *Mar. Pollut. Bull.* **2020**, *159*, 111517. [CrossRef] [PubMed]
2. Prata, J.C.; Silva, A.L.; Walker, T.R.; Duarte, A.C.; Rocha-Santos, T. COVID-19 Pandemic Repercussions on the Use and Management of Plastics. *Environ. Sci. Technol.* **2020**, *54*, 7760–7765. [CrossRef] [PubMed]
3. Roberts, K.P.; Phang, S.C.; Williams, J.B.; Hutchinson, D.J.; Kolstoe, S.E.; de Bie, J.; Williams, I.D.; Stringfellow, A.M. Increased personal protective equipment litter as a result of COVID-19 measures. *Nat. Sustain.* **2021**, *5*, 272–279. [CrossRef]
4. INE. 2020. Available online: https://www.ine.es/prensa/eiap_2020.pdf (accessed on 26 February 2023).
5. Abhilash; Inamdar, I. Recycling of plastic wastes generated from COVID-19: A comprehensive illustration of type and properties of plastics with remedial options. *Sci. Total Environ.* **2022**, *838*, 155895. [CrossRef] [PubMed]
6. Sun, X.; Liu, Z.; Shi, L.; Liu, Q. Pyrolysis of COVID-19 disposable masks and catalytic cracking of the volatiles. *J. Anal. Appl. Pyrolysis* **2022**, *163*, 105481. [CrossRef]
7. Dargahi, A.; Jeddi, F.; Ghobadi, H.; Vosoughi, M.; Karami, C.; Sarailoo, M.; Hadisi, A.; Mokhtari, S.A.; Haghighi, S.B.; Sadeghi, H.; et al. Evaluation of masks' internal and external surfaces used by health care workers and patients in coronavirus-2 (SARS-CoV-2) wards. *Environ. Res.* **2021**, *196*, 110948. [CrossRef]
8. Ilyas, S.; Srivastava, R.R.; Kim, H. Disinfection technology and strategies for COVID-19 hospital and bio-medical waste management. *Sci. Total Environ.* **2020**, *749*, 141652. [CrossRef]
9. Dharmaraj, S.; Ashokkumar, V.; Chew, K.W.; Chia, S.R.; Show, P.L.; Ngamcharussrivichai, C. Novel strategy in biohydrogen energy production from COVID-19 plastic waste: A critical review. *Int. J. Hydrogen Energy* **2021**, *47*, 42051–42074. [CrossRef]
10. Alabi, O.A.; Ologbonjaye, K.I.; Awosolu, O.; Alalade, O.E. Public and Environmental Health Effects of Plastic Wastes Disposal: A Review. *J. Toxicol. Risk Assess.* **2019**, *5*, 021. [CrossRef]
11. Siwal, S.S.; Chaudhary, G.; Saini, A.K.; Kaur, H.; Saini, V.; Mokhta, S.K.; Chand, R.; Chandel, U.; Christie, G.; Thakur, V.K. Key ingredients and recycling strategy of personal protective equipment (PPE): Towards sustainable solution for the COVID-19 like pandemics. *J. Environ. Chem. Eng.* **2021**, *9*, 106284. [CrossRef]
12. Zhao, X.; Klemeš, J.J.; You, F. Energy and environmental sustainability of waste personal protective equipment (PPE) treatment under COVID-19. *Renew. Sustain. Energy Rev.* **2021**, *153*, 111786. [CrossRef]
13. Wang, J.; Jiang, J.; Zhang, Y.; Meng, X.; Ragauskas, A.J. Upcycling disposable face masks into fuel range iso-alkanes through hydropyrolysis coupled with vapor-phase hydrocracking. *Energy* **2023**, *263*, 125843. [CrossRef]
14. Dogu, O.; Pelucchi, M.; Van de Vijver, R.; Van Steenberge, P.H.; D'Hooge, D.R.; Cuoci, A.; Mehl, M.; Frassoldati, A.; Faravelli, T.; Van Geem, K.M. The chemistry of chemical recycling of solid plastic waste via pyrolysis and gasification: State-of-the-art, challenges, and future directions. *Prog. Energy Combust. Sci.* **2021**, *84*, 100901. [CrossRef]
15. Sharma, G.; Upadhyay, E. Production of Hydrocarbon Liquid Fuels from waste Personal Protective Equipment (PPEs) through Pyrolysis. *Chemistryselect* **2022**, *7*, e202200356. [CrossRef]
16. Kartik, S.; Balsora, H.K.; Sharma, M.; Saptoro, A.; Jain, R.K.; Joshi, J.B.; Sharma, A. Valorization of plastic wastes for production of fuels and value-added chemicals through pyrolysis—A review. *Therm. Sci. Eng. Prog.* **2022**, *32*. [CrossRef]
17. Yoshioka, T.; Handa, T.; Grause, G.; Lei, Z.; Inomata, H.; Mizoguchi, T. Effects of metal oxides on the pyrolysis of poly(ethylene terephthalate). *J. Anal. Appl. Pyrolysis.* **2005**, *73*, 139–144. [CrossRef]
18. Ji, M.; Chen, L.; Que, J.; Zheng, L.; Chen, Z.; Wu, Z. Effects of transition metal oxides on pyrolysis properties of PVC. *Process. Saf. Environ. Prot.* **2020**, *140*, 211–220. [CrossRef]
19. Fadillah, G.; Fatimah, I.; Sahroni, I.; Musawwa, M.; Mahlia, T.; Muraza, O. Recent Progress in Low-Cost Catalysts for Pyrolysis of Plastic Waste to Fuels. *Catalysts* **2021**, *11*, 837. [CrossRef]
20. Li, C.; Yuan, X.; Sun, Z.; Suvarna, M.; Hu, X.; Wang, X.; Ok, Y.S. Pyrolysis of waste surgical masks into liquid fuel and its life-cycle assessment. *Bioresour. Technol.* **2021**, *346*, 126582. [CrossRef]
21. Chen, R.; Zhang, D.; Xu, X.; Yuan, Y. Pyrolysis characteristics, kinetics, thermodynamics and volatile products of waste medical surgical mask rope by thermogravimetry and online thermogravimetry-Fourier transform infrared-mass spectrometry analysis. *Fuel* **2021**, *295*, 120632. [CrossRef]
22. Hazan, M.A.; Mamat, M.S.; Ismail, I.; Hussein, M.Z.; Yaakob, Y. Fractionation of waste nitrile butadiene rubber (NBR) latex sludge. *AIP Conf. Proc.* **2019**, *2151*, 020012. [CrossRef]
23. Jung, S.; Lee, S.; Dou, X.; Kwon, E.E. Valorization of disposable COVID-19 mask through the thermo-chemical process. *Chem. Eng. J.* **2020**, *405*, 126658. [CrossRef] [PubMed]
24. Aragaw, T.A.; Mekonnen, B.A. Current plastics pollution threats due to COVID-19 and its possible mitigation techniques: A waste-to-energy conversion via Pyrolysis. *Environ. Syst. Res.* **2021**, *10*, 1–11. [CrossRef] [PubMed]
25. Park, C.; Choi, H.; Lin, K.-Y.A.; Kwon, E.E.; Lee, J. COVID-19 mask waste to energy via thermochemical pathway: Effect of Co-Feeding food waste. *Energy* **2021**, *230*, 120876. [CrossRef]

26. Brillard, A.; Kehrli, D.; Douguet, O.; Gautier, K.; Tschamber, V.; Bueno, M.-A.; Brilhac, J.-F. Pyrolysis and combustion of community masks: Thermogravimetric analyses, characterizations, gaseous emissions, and kinetic modeling. *Fuel* **2021**, *306*, 121644. [CrossRef]
27. Skrzyniarz, M.; Sajdak, M.; Zajemska, M.; Iwaszko, J.; Biniek-Poskart, A.; Skibiński, A.; Morel, S.; Niegodajew, P. Plastic Waste Management towards Energy Recovery during the COVID-19 Pandemic: The Example of Protective Face Mask Pyrolysis. *Energies* **2022**, *15*, 2629. [CrossRef]
28. Nawaz, A.; Kumar, P. Thermal degradation of hazardous 3-layered COVID-19 face mask through pyrolysis: Kinetic, thermodynamic, prediction modelling using ANN and volatile product characterization. *J. Taiwan Inst. Chem. Eng.* **2022**, *139*, 104538. [CrossRef]
29. Ali, L.; Kuttiyathil, M.S.; Altarawneh, M. Catalytic upgrading of the polymeric constituents in Covid-19 masks. *J. Environ. Chem. Eng.* **2022**, *10*, 106978. [CrossRef]
30. Lee, S.B.; Lee, J.; Tsang, Y.F.; Kim, Y.-M.; Jae, J.; Jung, S.-C.; Park, Y.-K. Production of value-added aromatics from wasted COVID-19 mask via catalytic pyrolysis. *Environ. Pollut.* **2021**, *283*, 117060. [CrossRef]
31. Yuwen, C.; Liu, B.; Rong, Q.; Zhang, L.; Guo, S. Self-activated pyrolytic synthesis of S, N and O co-doped porous carbon derived from discarded COVID-19 masks for lithium sulfur batteries. *Renew. Energy* **2022**, *192*, 58–66. [CrossRef]
32. Yang, W.; Cao, L.; Li, W.; Du, X.; Lin, Z.; Zhang, P. Carbon Nanotube prepared by catalytic pyrolysis as the electrode for supercapacitors from polypropylene wasted face masks. *Ionics* **2022**, *28*, 3489–3500. [CrossRef]
33. Ramalingam, S.; Thamizhvel, R.; Sudagar, S.; Silambarasan, R. Production of third generation bio-fuel through thermal cracking process by utilizing Covid-19 plastic wastes. *Mater. Today Proc.* **2023**, *72*, 1618–1623. [CrossRef]
34. Maity, S.; Srinivas, B.; Prasad, V.; Singh, A.; Dhar, G.M.; Rao, T. Studies on sepiolite supported hydrotreating catalysts. *Stud. Surf. Sci. Catal.* **1998**, *113*, 579–590. [CrossRef]
35. Deer, W.A.; Howie, R.A.; Zussman, J. *An Introduction to the Rock-Forming Minerals*, 2nd ed.; The Mineralogical Society: London, UK, 1992; Available online: http://pubs.geoscienceworld.org/minersoc/books/book/952/chapter-pdf/3751723/9780903056434_frontmatter.pdf (accessed on 9 January 2023).
36. Akbulut, A.; Kadir, S. The geology and origin of sepiolite, palygorskite and saponite in Neogene lacustrine sediments of the Serinhisar-Acipayam Basin, Denizli, SW Turkey. *Clays Clay Miner.* **2003**, *51*, 279–292. [CrossRef]
37. Sabah, E.; Çelik, M.S. Sepiolite: An effective bleaching adsorbent for the physical refining of degummed rapeseed oil. *J. Am. Oil Chem. Soc.* **2005**, *82*, 911–916. [CrossRef]
38. Suárez, M.; García-Rivas, J.; García-Romero, E.; Jara, N. Mineralogical characterisation and surface properties of sepiolite from Polatli (Turkey). *Appl. Clay Sci.* **2016**, *131*, 124–130. [CrossRef]
39. Song, N.; Hursthouse, A.; McLellan, I.; Wang, Z. Treatment of environmental contamination using sepiolite: Current approaches and future potential. *Environ. Geochem. Health* **2020**, *43*, 2679–2697. [CrossRef]
40. Foffi, R.; Savuto, E.; Stante, M.; Mancini, R.; Gallucci, K. Study of Energy Valorization of Disposable Masks via Thermochemical Processes: Devolatilization Tests and Simulation Approach. *Energies* **2022**, *15*, 2103. [CrossRef]
41. Remón, J.; Zapata, G.; Oriol, L.; Pinilla, J.L.; Suelves, I. A novel 'sea-thermal', synergistic co-valorisation approach for biofuels production from unavoidable food waste (almond hulls) and plastic residues (disposable face masks). *Chem. Eng. J.* **2022**, *449*, 137810. [CrossRef]
42. Fang, J.; Zhang, L.; Sutton, D.; Wang, X.; Lin, T. Needleless Melt-Electrospinning of Polypropylene Nanofibres. *J. Nanomater.* **2012**, *2012*, 382639. [CrossRef]
43. Gulmine, J.; Janissek, P.; Heise, H.; Akcelrud, L. Polyethylene characterization by FTIR. *Polym. Test.* **2002**, *21*, 557–563. [CrossRef]
44. Pinto, F.; Costa, P.; Gulyurtlu, I.; Cabrita, I. Pyrolysis of plastic wastes: 2. Effect of catalyst on product yield. *J. Anal. Appl. Pyrolysis* **1999**, *51*, 57–71. [CrossRef]
45. Tarach, K.A.; Góra-Marek, K.; Martinez-Triguero, J.; Melián-Cabrera, I. Acidity and accessibility studies of desilicated ZSM-5 zeolites in terms of their effectiveness as catalysts in acid-catalyzed cracking processes. *Catal. Sci. Technol.* **2017**, *7*, 858–873. [CrossRef]
46. Yousef, S.; Eimontas, J.; Striūgas, N.; Abdelnaby, M.A. Pyrolysis kinetic behaviour and TG-FTIR-GC–MS analysis of Coronavirus Face Masks. *J. Anal. Appl. Pyrolysis* **2021**, *156*, 105118. [CrossRef] [PubMed]
47. Yousef, S.; Eimontas, J.; Stasiulaitiene, I.; Zakarauskas, K.; Striūgas, N. Pyrolysis of all layers of surgical mask waste as a mixture and its life-cycle assessment. *Sustain. Prod. Consum.* **2022**, *32*, 519–531. [CrossRef]
48. Achilias, D.S.; Roupakias, C.; Megalokonomos, P.; Lappas, A.A.; Antonakou, E.V. Chemical recycling of plastic wastes made from polyethylene (LDPE and HDPE) and polypropylene (PP). *J. Hazard. Mater.* **2007**, *149*, 536–542. [CrossRef]
49. Donaj, P.J.; Kaminsky, W.; Buzeto, F.; Yang, W. Pyrolysis of polyolefins for increasing the yield of monomers' recovery. *Waste Manag.* **2011**, *32*, 840–846. [CrossRef]
50. Marongiu, A.; Faravelli, T.; Ranzi, E. Detailed kinetic modeling of the thermal degradation of vinyl polymers. *J. Anal. Appl. Pyrolysis* **2007**, *78*, 343–362. [CrossRef]
51. Silvério, F.O.; Barbosa, L.C.A.; Piló-Veloso, D. Pyrolysis as an analytical technique. *Quim. Nova* **2008**, *31*, 1543–1552. [CrossRef]
52. Serra, A.C.S.; Milato, J.V.; Faillace, J.G.; Calderari, M.R.C.M. Reviewing the use of zeolites and clay based catalysts for pyrolysis of plastics and oil fractions. *Braz. J. Chem. Eng.* **2022**, 1–33. [CrossRef]

53. Supriyanto; Ylitervo, P.; Richards, T. Gaseous Products from Primary Reactions of Fast Plastic Pyrolysis. *J. Anal. Appl. Pyrolysis* **2021**, *158*, 105248. [CrossRef]
54. Kumar, S.; Panda, A.K.; Singh, R. A review on tertiary recycling of high-density polyethylene to fuel. *Resour. Conserv. Recycl.* **2011**, *55*, 893–910. [CrossRef]
55. Noreña, L.; Aguilar, J.; Mugica, V.; Gutiérrez, M.; Torres, M. Materials and Methods for the Chemical Catalytic Cracking of Plastic Waste. *Mater. Recycl. Trends Perspect.* **2012**, 151–174. [CrossRef]
56. Almeida, D.; Marques, M.D.F. Thermal and catalytic pyrolysis of plastic waste. *Polímeros* **2016**, *26*, 44–51. [CrossRef]
57. Kass, M.D.; Armstrong, B.L.; Kaul, B.C.; Connatser, R.M.; Lewis, S.; Keiser, J.R.; Jun, J.; Warrington, G.; Sulejmanovic, D. Stability, Combustion, and Compatibility of High-Viscosity Heavy Fuel Oil Blends with a Fast Pyrolysis Bio-Oil. *Energy Fuels* **2020**, *34*, 8403–8413. [CrossRef]
58. Syamsiro, M.; Saptoadi, H.; Norsujianto, T.; Noviasri, P.; Cheng, S.; Alimuddin, Z.; Yoshikawa, K. Fuel Oil Production from Municipal Plastic Wastes in Sequential Pyrolysis and Catalytic Reforming Reactors. *Energy Procedia* **2014**, *47*, 180–188. [CrossRef]
59. Harussani, M.; Sapuan, S.; Rashid, U.; Khalina, A. Development and Characterization of Polypropylene Waste from Personal Protective Equipment (PPE)-Derived Char-Filled Sugar Palm Starch Biocomposite Briquettes. *Polymers* **2021**, *13*, 1707. [CrossRef]
60. Ouadi, M.; Jaeger, N.; Greenhalf, C.; Santos, J.; Conti, R.; Hornung, A. Thermo-Catalytic Reforming of municipal solid waste. *Waste Manag.* **2017**, *68*, 198–206. [CrossRef]
61. Martín-Lara, M.; Piñar, A.; Ligero, A.; Blázquez, G.; Calero, M. Characterization and Use of Char Produced from Pyrolysis of Post-Consumer Mixed Plastic Waste. *Water* **2021**, *13*, 1188. [CrossRef]
62. Vo, T.A.; Tran, Q.K.; Ly, H.V.; Kwon, B.; Hwang, H.T.; Kim, J.; Kim, S.-S. Co-pyrolysis of lignocellulosic biomass and plastics: A comprehensive study on pyrolysis kinetics and characteristics. *J. Anal. Appl. Pyrolysis* **2022**, *163*, 105464. [CrossRef]
63. Novak, J.M.; Cantrell, K.B.; Watts, D.W. Compositional and Thermal Evaluation of Lignocellulosic and Poultry Litter Chars via High and Low Temperature Pyrolysis. *BioEnergy Res.* **2012**, *6*, 114–130. [CrossRef]
64. Yaqoob, L.; Noor, T.; Iqbal, N. Conversion of Plastic Waste to Carbon-Based Compounds and Application in Energy Storage Devices. *ACS Omega* **2022**, *7*, 13403–13435. [CrossRef] [PubMed]
65. Azni, A.A.; Ghani, W.A.W.A.K.; Idris, A.; Ja'Afar, M.F.Z.; Salleh, M.A.M.; Ishak, N.S. Microwave-assisted pyrolysis of EFB-derived biochar as potential renewable solid fuel for power generation: Biochar versus sub-bituminous coal. *Renew. Energy* **2019**, *142*, 123–129. [CrossRef]
66. Xu, J.; Yu, J.; Xu, J.; Sun, C.; He, W.; Huang, J.; Li, G. High-value utilization of waste tires: A review with focus on modified carbon black from pyrolysis. *Sci. Total Environ.* **2020**, *742*, 140235. [CrossRef]
67. Yousef, S.; Eimontas, J.; Subadra, S.P.; Striūgas, N. Functionalization of char derived from pyrolysis of metallised food packaging plastics waste and its application as a filler in fiberglass/epoxy composites. *Process. Saf. Environ. Prot.* **2021**, *147*, 723–733. [CrossRef]
68. Wijesekara, D.A.; Sargent, P.; Ennis, C.J.; Hughes, D. Prospects of using chars derived from mixed post waste plastic pyrolysis in civil engineering applications. *J. Clean. Prod.* **2021**, *317*, 128212. [CrossRef]
69. Vanapalli, K.R.; Bhattacharya, J.; Samal, B.; Chandra, S.; Medha, I.; Dubey, B.K. Single-use LDPE—Eucalyptus biomass char composite produced from co-pyrolysis has the properties to improve the soil quality. *Process. Saf. Environ. Prot.* **2020**, *149*, 185–198. [CrossRef]
70. Bernardo, M.; Lapa, N.; Gonçalves, M.; Mendes, B.; Pinto, F.; Fonseca, I.; Lopes, H. Physico-chemical properties of chars obtained in the co-pyrolysis of waste mixtures. *J. Hazard. Mater.* **2012**, *219–220*, 196–202. [CrossRef]
71. Harussani, M.M.; Rashid, U.; Sapuan, S.M.; Abdan, K. Low-Temperature Thermal Degradation of Disinfected COVID-19 Non-Woven Polypropylene—Based Isolation Gown Wastes into Carbonaceous Char. *Polymers* **2021**, *13*, 3980. [CrossRef]
72. Miskolczi, N.; Ateş, F.; Borsodi, N. Comparison of real waste (MSW and MPW) pyrolysis in batch reactor over different catalysts. Part II: Contaminants, char and pyrolysis oil properties. *Bioresour. Technol.* **2013**, *144*, 370–379. [CrossRef]
73. Singh, E.; Kumar, A.; Khapre, A.; Saikia, P.; Shukla, S.K.; Kumar, S. Efficient removal of arsenic using plastic waste char: Prevailing mechanism and sorption performance. *J. Water Process. Eng.* **2019**, *33*, 101095. [CrossRef]
74. Dutta, N.; Gupta, A. Characterization and use of waste plastic char for removal of arsenic and COD from aqueous solution. *Int. J. Environ. Sci. Technol.* **2022**, 1–14. [CrossRef]
75. Solís, R.R.; Martín-Lara, M.; Ligero, A.; Balbís, J.; Blázquez, G.; Calero, M. Revalorizing a Pyrolytic Char Residue from Post-Consumer Plastics into Activated Carbon for the Adsorption of Lead in Water. *Appl. Sci.* **2022**, *12*, 8032. [CrossRef]
76. Alkan, M.; Tekin, G.; Namli, H. FTIR and zeta potential measurements of sepiolite treated with some organosilanes. *Microporous Mesoporous Mater.* **2005**, *84*, 75–83. [CrossRef]
77. Sabah, E.; Çelik, M. Interaction of Pyridine Derivatives with Sepiolite. *J. Colloid Interface Sci.* **2002**, *251*, 33–38. [CrossRef]

78. Justo, A.; Morillo, E. Structural alteration of pyrophyllite by dry grinding as studied by IR spectroscopy. *J. Mater. Sci. Lett.* **1994**, *13*, 915–918. [CrossRef]
79. Walczyk, A.; Karcz, R.; Kryściak-Czerwenka, J.; Napruszewska, B.D.; Duraczyńska, D.; Michalik, A.; Olejniczak, Z.; Tomczyk, A.; Klimek, A.; Bahranowski, K.; et al. Influence of Dry Milling on Phase Transformation of Sepiolite upon Alkali Activation: Implications for Textural, Catalytic and Sorptive Properties. *Materials* **2020**, *13*, 3936. [CrossRef]